Characteristic Scales of Chromospheric Oscillation Wave Packets

Scott W. McIntosh

Universities Space Research Association, CPSS, Seabrook, MD 20706.

Laboratory for Astronomy and Solar Physics,
NASA Goddard Space Flight Center, Mailcode 682.3, Greenbelt, MD 20771.

scott@grace.nascom.nasa.gov

and

Darren G. Smillie[1]

Laboratory for Astronomy and Solar Physics,
NASA Goddard Space Flight Center, Mailcode 682.3, Greenbelt, MD 20771.

darren@grace.nascom.nasa.gov

ABSTRACT

We use wavelet transforms to study the characteristic time scales of chromospheric oscillation "wave packets" that are observed in Transition Region and Coronal Explorer (TRACE) ultraviolet continuum image timeseries. Using several datasets we investigate the statistical, spatial and temporal intermittence of the number, duration, mean frequency and delay ("wait-time") between wave packets in the timeseries data. Further, we demonstrate that these characteristic values are consistent with newly developed pictures of the wave-mode suppression and conversion by the chromospheric magnetic "canopy". We propose that this wavelet transform analysis will permit rudimentary structure diagnosis of the chromosphere and a full (temporal and spatial) investigation connecting chromospheric oscillation wave-packets to their sources in the photosphere.

Subject headings: Sun: chromosphere - Sun: atmospheric motions - Sun: magnetic fields - Sun: transition region - Sun: UV radiation

1. Introduction

Oscillations observed in the upper photosphere, chromosphere and the transition region plasmas have been noted to interact symbiotically with the atmospheric plasma topography in which they are observed (see, e.g., McIntosh et al. 2001; Krijger et al. 2001; McIntosh & Judge 2001; McIntosh et al. 2003, and references therein). These oscillations are generally acoustic in nature and stem from either the superposition and subsequent interference of global p-modes that propagate in the Sun's interior (e.g., White & Cha 1973; Cha & White 1973) or the thermodynamic collapse of granular cells (Rast 1999; Skartlien & Rast 2000) and have received considerable attention as one possible source of energy and support for the ambient quiet

[1]Current Address: Department of Physics, Blackett Laboratory, Imperial College London, London SW7 2BW, UK.

chromosphere and corona (see the excellent review of Rutten 2003). They manifest themselves in the Sun's outer atmosphere as small, isolated, but systematic, "packets" of as few as one, two or three wave periods which lose coherence or switch off and wait for a measurable amount of time before the next packet occurs. We will primarily focus on the analysis of these "wave packets[2]" in the chromosphere where they are simply dubbed chromospheric oscillations.

To date, much of the analysis performed on chromospheric oscillations has been based on Fourier techniques which, more or less by definition, assume that the observed wave modes are persistent spatially and temporally over the duration of the observation. The source, or "piston", of chromospheric oscillations dictates the analysis method required since both granular collapse and the local interference of multiple, global p-modes are obviously highly intermittent in time and space, Fourier analysis is inadequate and we should instead employ a method that can capture the full temporal and spatial dependence of chromospheric oscillations. We should, however, not overlook the significant insight into the nature and propagation of chromospheric oscillations provided by Fourier analysis (see, e.g., Rhodes, Ulrich & Deubner 1979; Lites et al. 1982; Deubner & Fleck 1990, including most of the papers cited previously). It is exactly the spatial and temporal intermittence of chromospheric oscillations and their (unresolved) generation mechanism that makes their analysis amenable to a multi-scale, time-frequency wavelet transform analysis as a natural extension to the standard (Fourier) frequency domain analysis. Put simply, wavelet transforms allow the localization of the packet in the frequency and time domains simultaneously with a small trade-off in accuracy (see, e.g., Torrence & Compo 1998). In the following sections we will discuss the application of wavelet transforms to chromospheric oscillation analysis and explore some of the temporally and spatially "local" features that result.

In Sect. 2 we discuss the data and reduction methods that we apply to the Transition Region and Coronal Explorer (Handy et al. 1999, TRACE) UV image timeseries used in this paper. In Sect. 3 we present and demonstrate the application of wavelet transforms to these data and define the packet "parameters" that we will employ to characterize, count and time the chromospheric packets in eight illustrative TRACE datasets: the packet mean frequency, ν_X, the packet duration, D_X, the packet number, N_X and the packet wait time Δt_X, where X denotes the region being studied, network ($X = N$) or inter-network ($X = I$). Physical attributes of the chromospheric oscillations (and their sources) are readily attached to the defined packet parameters. Specifically $\hat{N_X}$, the number of packets per hour, indicates the frequency of piston occurrence or p-mode interference. Likewise, the wait time Δt_X can be thought of as the time between piston actions or constructive interference events and the packet duration as the coherent life-time of the piston or the coherence time of the impinging p-modes. In Sect. 4 we tabulate the characteristic features of each of those datasets and present, in Sect. 4.1, examples to illustrate the spatial distribution of packet parameters. Indeed, to extend this work and to point to future investigations of this kind we present, in Sect. 4.2, an investigation into the vertical nature of the packet parameters in a typical, well studied, multi-wavelength (multiple formation temperature) joint TRACE and Solar and Heliospheric Observatory (SOHO; Fleck et al. 1995) Joint Observing Program (JOP) 72 dataset. To close, in Sect. 6, we will discuss these results and place them in context with other chromospheric oscillation investigations of the solar atmosphere that can be pursued in the future (Sect. 5).

Through the combined analysis of TRACE, Solar Ultraviolet Measurements of Emitted Radiation

[2]For the purpose of this paper we define a "wave packet" as a short-duration, multi-frequency packet of oscillations in timeseries observations of the solar chromospheric plasma. For brevity, from this point onward we will refer to wave packets simply as packets.

(SOHO/SUMER; Wilhelm et al. 1995) and Michelson Doppler Imager (SOHO/MDI; Scherrer et al. 1995) timeseries data we demonstrate that the packet parameter values are consistent with newly developed pictures of how the chromospheric "canopy" influences the observed signal and may open a path to performing a rudimentary topographic diagnosis. Further, we propose that a wavelet based analysis of chromospheric oscillations may help us to resolve issues of temporal variations in the observation of the plasma's time-evolving topography[3] to track and study the variation of individual packets as they travel from creation to (possible) dissipation.

2. Data and Reduction

To characterize the nature of these packets in the outer solar atmosphere we will perform the wavelet analysis for an archive of timeseries data from TRACE which have co-temporal magnetic topological context provided by MDI. From May 1998 until August 2001 there are eight datasets of sufficient duration ($\geq$ 1 hour) and fixed, short TRACE cadence ($\sim$ 15 seconds) to perform this study. More often than not, such observations were the result of carefully designed SOHO Joint Observing Programs (JOPs; more specifically JOP26, JOP40, JOP72 and JOP97) using multiple instruments on the SOHO spacecraft to complement the TRACE observations (see, e.g., Judge et al. 2001). This relatively small set of observations represents a wide range of solar plasma topographies; from sunspots to (very quiet) disk center inter-network observations.

We use the data reduction method outlined in Sect. 2 of Krijger et al. (2001) to investigate the timeseries of the TRACE continuum bandpass images. The first step in the analysis of the data involves the co-alignment of the initial TRACE image and MDI magnetogram of the timeseries. Then we form data cubes for the TRACE timeseries, D_λ(x,y,t), with each frame co-aligned with the previous one with sub-pixel accuracy (see, e.g., McIntosh et al. 2003). This image correlation process ensures that the data cubes are as insensitive as possible to the effects of contamination from cross-talk in the signal produced by solar rotation. In the following sections we predominantly limit our discussion to the analysis of TRACE 1700Å image timeseries because of their relatively high feature contrast and signal-to-noise ratio (T.D. Tarbell 2003 - Private Communication) and, as we show in Sect. 4.2, that the measured packet descriptions are consistent in each of the three TRACE continua (1550, 1600 and 1700Å).

Once the images are co-aligned, we spatially re-bin the data-cubes into $1'' \times 1''$ (i.e., 2×2 TRACE pixels) blocks ensuring an accurate spatial description of the packet with sufficient signal-to-noise to isolate spatially "local" events without smearing the oscillation excessively. Judge et al. (2001) demonstrated (in Sect. 3.3.3 and in Fig. 7 of their paper) that the spatial coherence length-scale observed in various JOP72 TRACE chromospheric oscillations studies was of the order of $1''$.

3. Morlet Wavelet Analysis

Figure 1 illustrates the key features and measures used in this paper to characterize packets in the TRACE 1700 Å continuum timeseries observations following the application of the Morlet[4] wavelet transform

[3]Of course, when we refer to the plasma topography we mean the entire plasma structure; including magnetic field topology (the chromospheric "canopy") and the plasma in which it is threaded.

[4]We note that other wavelet bases are available and may modify the results presented slightly but the Morlet wavelet best represents the types of sinusoidal oscillations present in our data (see, e.g., O'Shea, Muglach & Fleck 2002).

discussed in Torrence & Compo (1998). This characterization defines when packets statistically exist in a times-series, how many packets there are over the duration of the timeseries, how long they last, how much time passes between packets and what the mean frequencies of the packet oscillations are. The position of the white asterisk in the top right thumbnail of the TRACE FOV marks the location of the pixel timeseries that is presented as an example in panel a). At first glance, the timeseries would appear to present a regular oscillation with a period of about 4 minutes, but the signal seems to be temporally intermittent with sizeable breaks from regular periodic oscillation.

In panel b) we show the wavelet power spectrum of this pixel timeseries and the regions of high wavelet power are clearly visible. We also show the "cone-of-influence" (black cross-hatched area under the curve) which marks the region of uncertainty caused by the finite length of the timeseries (its shape is a function of the length of the timeseries and the chosen wavelet basis). Many of the regions of high power have greater than 95 % statistical confidence and are placed inside of thick black contours. The power that is contained within each of these closed 95 % confidence contours *and* is completely outside the cone-of influence defines one instance of the multi-frequency packets that we are studying in this paper. When we make the further restriction that we are interested in packet frequencies between 3 and 8 mHz[5] we can see that there are two "statistically significant" regions of power in this particular, hour long pixel timeseries.

In panel c) we show the "global wavelet power spectrum" (GWPS, as defined by Torrence & Compo 1998) which is the mean wavelet power averaged over time and is the feature most comparable to the Fourier power spectrum of the timeseries (exception that it is significantly smoother). From the GWPS we are able to define and measure the peak period 4.13 minutes (frequency of ∼4.00 mHz) of the packets present in the 3-8 mHz frequency band. Similarly, the GWPS can be integrated over the same range of frequencies to obtain a measure of the average oscillatory power present in that spatial pixel. We note that the lower peak in the GWPS can be neglected since it belongs to a packet that is predominantly within the cone-of-influence and is also not statistically significant, each of which is a criterion for rejection.

The lowest panel of Fig. 1, d), shows the 3-8 mHz frequency averaged wavelet power as a function of time. This is the object that allows us to measure the time-related parameters of the packets present; the packet duration and the packet "wait-time" (the time between packets) along with the peak packet power. We note that the inclusion of the longer "unfinished" (yellow) packet wait-times cause a net under-estimation of the mean wait-time over the duration of the timeseries. The dashed line in the plot indicates the frequency averaged 95% confidence level contours of panel b); the intersection of this line with the power curve marks the temporal boundaries of the packets. These intersections are marked as finely cross-hatched areas on the panel and are similarly traced onto panel a). Visually cross-referencing these cross-hatched regions with the two statistically significant wavelet power regions in panel b) provides a check for the method.

We have now defined several parameters of the packets present in the 1700Å TRACE continua that we will use in the following section, namely the packet mean frequency, ν_X, the packet duration, D_X, the packet number, N_X, and the packet wait time Δt_X(the subscript X will be used to distinguish spatially between the network, $X = N$, and inter-network, $X = I$, regions). To complement these quantities and to normalize for observations of different lengths we introduce the packet number per hour, $\hat{N_X}$, and the number of periods per packet, $\hat{P_X}(= D_X \nu_X)$. As we have discussed above, the systematic behavior of these

[5]We note that our choice of the wide 3-8 mHz frequency band (including evanescent and propagating wave frequencies in the chromosphere) allows spatial study of packet frequencies with sufficient contrast to identify and evaluate network and inter-network regions in Sect. 4.1; study of smaller, more carefully selected frequency bandpasses is the subject of a future paper (McIntosh 2004).

diagnostic parameters in concert will provide us with the potential to investigate the temporal and spatial characteristics of chromospheric oscillations.

4. Results

The packet parameters defined above provide us with a means to characterize chromospheric oscillation timeseries data temporally, spatially and statistically. In Figure 2 we present details of the packet parameter histogram samples from the longest timeseries available, that of the JOP97 sunspot data, September 22, 2000 (set # 7; also discussed in Muglach & Hofmann 2003). At the top of this figure we show, from left to right, the imaging context for the timeseries in the form o f the time averaged SOHO/MDI $B_{||}$ and TRACE 1700Å continuum intensity maps. Between these two images we show the masks that we have defined to delineate the inter-network ("IN"; $\|B_{||}\| < 10$ Mx cm^{-2}; white), network ("N"; $20 < \|B_{||}\| < 400$ Mx cm^{-2} ; light grey), an intermediate buffer between them ("O"; $10 < \|B_{||}\| < 20$ Mx cm^{-2} ; dark grey) and the sunspot ("S"; $\|B_{||}\| > 400$ Mx cm^{-2}; black) regions; please note that due to signal-to-noise problems we omit data from the latter (instead see O'Shea, Muglach & Fleck 2002, who study waves in sunspot umbrae). In the lower set of panels we show the packet parameter distributions for each of these regions; a) the packet frequency ν_X, b) the number of packets N_X, c) the packet duration D_X and d) the packet wait-time Δt_X. The gray shaded histograms in each panel show the packet parameter distributions for *all* spatial pixels (again, except those of the sunspot). Contained within these shaded histograms are the network (solid black line) and inter-network (solid white line) parameter distributions which allow us to visualize the spatial differences in the parameters from a statistical standpoint.

Clearly, the all-pixel packet parameter distributions (in this case) are bimodal and the differences between the distributions from the network and inter-network regions are evident. We see (in panel a) that the mean frequencies of the packets in the network is 3.74 mHz while it is 5.06 mHz in the inter-network region; a difference that has been known for some time (Liu & Sheeley 1971). We can also see (panel b) that there are ∼1.5 more packets in inter-network regions than there are in network regions over the duration of timeseries. The packets themselves are of very similar duration (panel c), with distribution means separated by only one minute in each region. This implies that there are a different number of individual oscillations ($\hat{P_X}$) within each packet in the network (∼1.5 periods) and inter-network (∼2.3 periods) regions. Likewise, in network regions, there are on average fewer packets which have a shorter duration; so it is reasonable to expect that we would have to wait longer for each packet to come along. Indeed, this is demonstrated in panel d) where the mean network packet "wait-time" is some four minutes longer. Physically speaking, the parameter distributions in this dataset provide a valuable insight into the nature of chromospheric oscillations in what are assumed to be vastly different magnetic environments. The excess of packet suppression and the short coherence times (small number of periods per packet) in network regions are indicative of the well known influence of the magnetic field on the oscillation's piston mechanism in the chromospheric network relative to that in the inter-network.

In Table 1 we present the details of the analysis of the eight TRACE 1700 Å continuum timeseries datasets. Each quantity presented is the mean value of the distribution for that region at $1'' \times 1''$ spatial resolution and each has a corresponding deviation but for the purpose of limiting the size of this table are omitted[6]. We can see that some of the packet parameter variations have a dependence with the MDI

[6]We refer the reader to Tab. 2 and Fig. 3 which have typically representative values of the distribution deviation for each of the timeseries presented. Table 2 also shows values of the packet parameters for the other TRACE UV continuum bandpasses.

unsigned network line-of-sight magnetic flux density B^* (units; Mx cm^{-2}). We see that the ν_X are typically lower in the network regions, ∼3.4 mHz, than in the inter-network regions, ∼4.0 mHz, but the values of ν_I appear to scale with B^*. We also see that the packet duration and wait-time vary inversely (long duration - short wait-time and vice versa). There are considerably more packets in the inter-network regions and the number per hour ($\hat{N_X}$) is dependent on the mean field strength. Similarly, the number of peak-to-peak oscillations per packet is approximately uniform in the inter-network regions at ∼2.5 while, in the network regions, it decreases from 2.5 in set #4 to 1.5 in set #7 as B^* increases, i.e., there are fewer pulses per packet in strong network regions. This effective quenching of chromospheric oscillations, and oscillatory power has been widely discussed, both by the present author in previous publications and in, for example, Title et al. (1992).

From top to bottom Fig. 3 illustrates the dependence of the mean values (and variances) of ν_X, $\hat{N_X}$, D_X, Δt_X and $\hat{P_X}$ with B^* of the network (dark dots) and inter-network (light dots) columns of Tab. 1 along with their respective least-squares linear fits and gradients (M_X). Panel a) shows that ν_X in the network regions is invariant with B^* (within the error bars) while, in inter-network regions, the value of ν_X shows a small increase, although we note the use of a linear fit in this case is probably inaccurate because most of the growth occurs from $B^* \geq 75$ Mx cm^{-2}. The growth of ν_I as B^* increases is indicative of a contamination of inter-network structure by the lowering and expansion of the chromospheric "canopy" and we will discuss this further below. In panels b) and c) we see that the linear fits to $\hat{N_X}$ and D_X are effectively parallel to one another. In both cases this suggests that the degree by which the packet generation mechanism is suppressed or is truncated increases with B^* no matter what region we are considering. This, again, points to the influence of the network magnetic field strength and its expanding outward topology into the inter-network regions. In panel d) it is clear that the network wait-time does not vary with B^*. Hence, the separation between oscillations is independent of B^* inside network elements. However, the inter-network wait-times increase with B^* which is consistent with the decreasing packet durations and, from panel e), the fact that the number of periods per packet is effectively invariant. Likewise, in panel e), we suggest that the decrease in network periods per packet with B^* is due to the invariant wait-time of panel d) and the decreasing packet durations of panel c).

The details and relationships of the packet parameters presented in Tab. 1 and Fig. 3 point to global p-mode interference as the local piston responsible for the chromospheric oscillation packets observed. The decrease in the number of packets, the anti-correlated variations in packet duration and wait-time (particularly in inter-network regions) and all of the parameters' variations with B^* point to a degree of systematic regularity in the piston responsible, irrespective of where they are observed.

4.1. Spatial Behavior

We explore the spatial distributions of the packet parameter to expand upon some of the relationships discussed above. As examples we will use datasets from the opposite ends of the topographic spectrum, the "weak-field" case of 26 February 1999 (set # 4) in Fig. 4 and again, the sunspot, "strong-field" case of 22 September 2000 (set # 7) in Fig. 5.

In the center and right columns of Figs. 4 and 5 we demonstrate the spatial behavior of the packet parameters beside those of the mean TRACE 1700Å continuum intensity (top left panel) and MDI $B_{||}$ (bottom left panel). The solid black contour shown on each panel marks the boundary between the network and inter-network plasma as defined above. Several features are immediately clear as we might expect from

the discussion above. The lower packet frequencies inside the network regions are contained within these contours (center top panel). Similarly, in network regions, there appear to be fewer packets (top right panel), which is consistent with the fact that the wait time is significantly longer there (bottom right panel). Despite all of these relatively strong spatial correlations the packet duration (center bottom panel) shows little dependence on where the packets are located. On comparing the packet frequency panels we can clearly see, as was noted above, that the inter-network frequencies in set # 7 ($\sim$ 5.1 mHz) are significantly different from those in set # 4 $\sim$4.0 mHz which could very much be considered as a typical "quiet" internetwork oscillation frequency in the TRACE 1700 Å bandpass. Indeed, we can also see in Fig. 5 that there is a relatively smooth transition from network to inter-network frequencies that is indicative of the canopy effects on chromospheric oscillations that were demonstrated in the figures of Krijger et al. (2001) and McIntosh & Judge (2001).

From Fig. 5 we see that there is a broad enough range of magnetic flux densities to quantitatively explore the broad, bimodal, all-pixel parameter distributions shown in Fig. 2 and the influence of the extended magnetic "canopy" on the packet parameters. In Fig. 5 we show scatter plots of packet frequency (panel a), number (panel b), duration (panel c) and wait-time (panel d) versus the corresponding (coaligned) absolute values of $B_{||}$ ranging from 0 to 40 Mx cm^{-2}. In each panel the solid line corresponds to the location of the maximum scatter density at each value of $|B_{||}|$ and we can clearly see that there is a smooth transition from the true inter-network[7] to the effectively constant network values at about 20 Mx cm^{-2}. The gray shaded regions of smooth transition we attribute to the magnetic "canopy".

4.2. Multi-wavelength Wave Packet Analysis

In addition to providing SOHO/MDI and TRACE timeseries observations of a (very) quiet region near disk center dataset # 4 has complementary SOHO/SUMER timeseries observations, allowing us to analyze the wave packet parameters over a large vertical extent, effectively "tracking" their average behavior from the photosphere through the chromosphere and into the transition region plasma with the gradual decay of the inter-network magnetic field[8]. The Morlet wavelet techniques discussed above were applied to the timeseries of TRACE (1700Å, 1600Å, 1550Å), MDI ($V_{||}$) and several SUMER continua and Doppler velocities derived from spectral lines (1195Å Continuum; N I 1199.55Å, 1200.22Å; Si II 1197.40Å; Si III 1206.51Å) in a inter-network region of the TRACE FOV that was chosen to both optimize the signal-to-noise ratio of the SUMER data and to avoid the so-called "magnetic shadow" which has already been demonstrated to suppress oscillatory behavior (McIntosh & Judge 2001).

The raw SUMER data have been spatially rescaled to 2 pixel ($2 \times 1''$, along the slit) blocks to more accurately describe the spatial distribution of the packets and improve the signal-to-noise ratio. This re-binning is below the SUMER spatial correlation length-scale of $5''$ that was derived by Judge et al. (2001). During these observations the SOHO spacecraft was rolled at 119.2° to the solar North-South line[9] and so SUMER was not correcting its observations for solar rotation, as a result the SUMER spectroscopic data drift spatially, but steadily, by several arcseconds ($<10''$) over the duration of the observations. Due to the

[7]At this stage we should note that our defined inter-network magnetic field bounds are generous; we should ideally have $|B_{||}| \sim 0$ Mx cm^{-2}. By using too broad a range in $B_{||}$ the distributions of inter-network parameters are artificially wide in some cases (cf. set # 7).

[8]Similar analysis of such datasets have been made but were restricted to sunspot umbrae or individual strong network elements (see, e.g., O'Shea, Muglach & Fleck 2002; McAteer et al. 2003).

[9]Please see Fig. 1 of Judge et al. (2001) for SUMER pointing context.

extended "pancake" structure of the oscillations that arises from the 5″ spatial correlation length-scale and the fact that we do not expect the packets present to be longer than 20 minutes in duration (drift of ∼2.5″ at disk center), we have not attempted to remove the effects of rotation in the SUMER data and potentially introduce additional spectral, frequency-dependent noise in our calculations. Previously determined Fourier transform results using these data (Judge et al. 2001) have shown that the mean frequency of chromospheric waves in inter-network regions increases with height 5-minute periods at the bottom of the chromosphere to 3-minute periods at the top. We therefore expected to see the peak packet frequency follow this trend and, as a consequence, the duration of the wave packets decrease slightly with the wait time increasing correspondingly. The number of packets (N_I) and the number of periods per packet are expected to remain relatively constant in this weak inter-network region because they only display a weak dependence on $B_{||}$ from Tab. 1 and Fig. 3.

From Tab. 2, the following relationships are clear. As predicted, both the packet number and number of periods per packet are effectively conserved across all heights within the determined error bars. The peak frequency of the oscillations within each packet shows a gradual increase with height. The period decreases from approximately 5 minutes for the MDI $V_{||}$ data to approximately 3.5 minutes in the Si III line, arguably the line formed highest in our sample. With the increase in packet frequency with height we would expect to see a decrease in the packet duration as is observed, although the SUMER data shows slightly shorter durations than we might have expected from the results above. However, the packet wait-times do not correspond as expected with the durations - we expect that as the packets become shorter the time between packets must increase *if* the packet number is conserved. In fact, little variation in wait time is observed (note the large error bars associated with the wait times). Finally, we see that the 1550Å, 1600Å and 1700Å TRACE UV continua give extremely close and consistent values for each of the wave packet parameters as we have anticipated as they are not significantly separated in height, justifying our earlier focus on the analysis of 1700Å TRACE data only.

In general, there are significantly larger errors associated with the packet parameters derived from the SUMER lines than those from the MDI or TRACE timeseries; explainable by the high noise content of the SUMER data and the small number of pixels available to sample (we have used the inter-network regions of the entire TRACE/MDI FOV). Effects of this could include "washing out" of oscillations in true wave packets or, conversely, sections of noise could be mistaken for true oscillations. In both cases we expect a reduction in duration (e.g., observing a lengthy "noise packet" is unlikely O'Shea, Muglach & Fleck 2002), while these combined effects could also explain the slight increase in packet number observed. This increase in packet number will, to some extent, cancel out the effect of reduced duration on the length of the wait times, which may explain their apparent lack of variation. There is a clearly a motivation to obtain and analyze more datasets where SUMER observations are coordinated with those of TRACE and MDI, in order to investigate the vertical relationships of the wave packet parameters.

5. Future Considerations

Several of the features discussed above require some further investigation that is both beyond the quality of the data presented and the scope of this paper. By far the most important of these is the potential to isolate, quantify, understand and actually connect the observed chromospheric oscillations to the piston that generates them. Much of the data available today, including those presented here, are of insufficient spatial resolution to address the connection of oscillation and generator, but the method detailed is very applicable to the task of looking for "local" wave and propagation (refraction, reflection and conversion) effects. By

studying wave-packets in the Earth's oceans Liu (2000) has constructed simple cross-wavelet correlation, coherence and phase differences relationships that may help us understand the piston mechanism better.

Other questions exist. What role does wave-mode interference play in the magnetic canopy in dictating what we observe there? The simulations of Rosenthal et al. (2002); Bogdan et al. (2002, 2003) demonstrated the canopy as a realm where magneto-atmospheric wave-modes of different frequencies and magnetic influences can impinge and beat on one-another readily. Similarly, the suppression of packet number, short packet duration and oscillatory power by strong network, or plage, magnetic fields has been noticed and again we ask what is the role does the plasma topography play in this phenomenon. Is this a situation where interference is important again, where short quasi-periodic pulses of constructive interference "mislead" the wavelet analysis or is the plage region a tangled mess of low-lying, high-pitch-angle field structures that suppress wave-modes (see observational and simulation examples in McIntosh et al. 2001; McIntosh & Judge 2001; Rosenthal et al. 2002)?

We plan to acquire high-cadence "synoptic" observations in the 1700, 1600Å UV continua at a fixed high cadence (of the order of 10s) to build a catalog of different solar topographies for comprehensive study of wave-packets as well as other spatial and spectral phenomena as a first step.

6. Discussion

In the preceding sections we have seen that chromospheric oscillations are not persistent in time, they last on average only a few periods before dying out, only to re-appear some time later. These short-duration bursts of oscillation are clearly identifiable as being multi-frequency packets in the timeseries observations. The localization of the packets in frequency and time makes their analysis readily amenable to wavelet transforms. We have seen that the characteristic scales of oscillation intermittence are tied to the magnetic environment in which they are generated (either through granular collapse or global p-mode interference). In an effort to understand and quantify these ties we have parameterized the occurrence of chromospheric oscillation wave-packets through their mean frequency, duration, number and wait-time. In Sect. 4 we have explored the statistical and spatial behavior of the wave-packet parameters and demonstrated their dependence and variation with one another and with the magnetic topology that threads the chromospheric plasma.

We show, in Fig. 7, qualitative (idealized axisymmetric) cartoon visualizations of the plasma topography in the strong and weak-field cases for comparison with those presented in Figs. 4 and 5, and with their two-dimensional counterpart presented in Gabriel (1976). This figure is meant to explain the role of the plasma topography in dictating the wave-packet frequency and subsequently the other wave-packet parameters. The spatial (x-y) scales of each cartoon are different; with the weak-field case (left; 1 Mm) having twice the spatial scale of the strong-field case (right; 10 Mm). We assume that the vertical (z) scales are the same (1 Mm). In each cartoon we show a representative magnetic field topology (multi-colored solid lines), an plasma-$\beta = 1$ iso-contour (shaded gray region), an estimate of the vertical position of the TRACE 1700Å continuum formation layer (green gridded surface) and the total atmospheric pressure (gas pressure + magnetic pressure) isobars which correspond to the topographic locations where 5-minute (3.3 mHz; solid thick black line), 4-minute (4.2 mHz; solid thick green line) and 3-minute (5.6 mHz; solid thick blue line) period waves are predominant. Notice the topological differences in each cartoon, the differing horizontal spread of the field, and the net effect that the strength of the magnetic field plays in contributing to the lowering of the characteristic period iso-surfaces and the plasma-$\beta = 1$ iso-contour, i.e. the magnetic canopy,

into the inter-network regions.

We propose that the intersection of the TRACE 1700Å formation surface and the characteristic period iso-surfaces determines the frequency of wave packets that are observed and can explain some of the features observed in the figures and tables of this paper. Again, we use the inter-network regions of sets #4 and 7 as examples to illustrate this proposition. Typical chromospheric oscillations present in TRACE 1700Å bandpass timeseries of the inter-network have a four-minute period, compare this to left side of Fig. 7 where the formation surface samples the four-minute pressure iso-contour just outside out of the network element core and out into inter-network. In Fig. 5, however, we saw that the inter-network frequencies were approaching those of three-minute waves, but we would expect to find three-minute waves at significantly higher levels of the typical inter-network atmosphere, say at SUMER continuum levels like those discussed by McIntosh et al. (2001). It would appear that the atmosphere "shrink-wraps" itself around the network elements, thus significantly altering the total pressure structure of the atmosphere around the magnetic element. How far that influence is carried is determined by the strength of the magnetic field in the network elements; the stronger the flux, the more far-reaching its effect on the inter-network plasma.

Through the combined analysis of TRACE, SOHO/SUMER and SOHO/MDI timeseries data, we have demonstrated that these characteristic wave-packet parameters are consistent with current pictures of wave interaction with the chromospheric "canopy". The connection of wave-packet parameters and the underlying magnetic field makes this technique into a basic structural diagnostic of the chromospheric plasma. Further, the timing and spatial structure of the wave-packet parameters point to global p-mode interference as the chromospheric oscillation wave-packet generation mechanism in the lower regions of the atmosphere although this, for the reasons mentioned above, must be investigated further.

The authors would like to thank Dr. Rob Rutten for taking the time to help us greatly improve the content and clarity of this paper. DGS acknowledges the support of the NASA GSFC/LASP summer intern program. SWM acknowledges the support of the GSFC SDAC and NASA's Living With A Star Program and would also like to than Prof. John Lawrence and Dr. Alex Young for discussions on wavelet transform applications. Finally we thank the TRACE instrument team for making their data available and agreeing to conduct a synoptic 1600/1700 observation program.

REFERENCES

Bodgan, T. J., Rosenthal, C. S., Carlsson, M., et al. 2002, Astron. Nachr, **323**, 196

Bodgan, T. J., Rosenthal, C. S., Carlsson, M., et al. 2003, *In Press*, ApJS

Cha, M. Y. & White, O. R. 1973, Solar Phys., **31**, 23

Deubner, F.-L. & Fleck, B. 1990, A&A, **228**, 506

Fleck, B., Domingo, V., Poland, A. I. 1995, *The SOHO mission*, Dordrecht: Kluwer

Gabriel, A. H. 1976, Phil. Trans. R. Soc. Lond. A, **281**, 339

Handy, B. N., Acton, L. W., Kankelborg, C. C., Wolfson, C. J., Akin, D. J. et al. 1999, Solar Phys., **187**, 229

Judge, P. G., McIntosh, S. W. 1999, Solar Phys., **190**, 331

Judge, P. G., Tarbell, T. D., Wilhelm, K. 2001, ApJ, **554**, 424

Krijger, J. M., Rutten, R. J., Lites, B. W., et al. 2001, A&A, **379**, 1052

Lites, B. W., Chipman, E. G. & White, O. R. 1982, ApJ, **253**, 367

Liu, P. C. 2000, In *Advances in Coastal and Ocean Engineering Book Series*, P. L. F. Liu (Ed.), Vol. 6, World Scientific, 57

Liu, S. Y. & Sheeley, N. R. 1971, Solar Phys., 20, 282

McAteer, R. T. J., Gallagher, P. T., Williams, D. R. 2003, ApJ, **587**, 806

McIntosh, S. W., Bogdan, T. J., Cally, P. S., et al. 2001, ApJ, **548**, L237

McIntosh, S. W., Judge, P. G. 2001, ApJ, **561**, 420

McIntosh, S. W., Fleck, B., Judge, P. G. 2003, A&A, **405**, 706

McIntosh, S. W. 2004, *In preparation*

Muglach, K. & Hofmann, A. 2003, *Submitted to* A&A

O'Shea, E., Muglach, K., Fleck, B. 2002. A&A, **387**, 642

Rhodes, E. J., Ulrich, R. K., Deubner, F.-L. 1979, **227**, 629

Rosenthal, C. S., Bodgan, T. J., Carlsson, M., et al. 2002, ApJ, **654**, 508

Rutten, R. J. 2003, In *Turbulence, Waves, and Instabilities in the Solar Plasma*, R. von Fay- Siebenbürgen, K. Petrovay, J.-L. Ballester, M. Aschwanden (Eds), Procs. NATO Advanced Research Workshop, Budapest, 2002. Kluwer, Dordrecht.

Scherrer, P. H., Bogart, R. S., Bush, R. I., Hoeksema, J. T., Kosovichev, A. G. et al. 1995, Solar Phys., **162**, 129

Rast, M. P. 1999, ApJ, **524**, 462

Skartlien, R., Rast, M. P. 2000, ApJ, **535**, 464

Title, A. M., Topka, K. P., Tarbell, T. D., et al. 1992, ApJ, **393**, 782

Torrence, C., Compo, G. P 1998, Bull. Am. Met. Soc., **79**, 61

White, O. R. & Cha, M. Y. 1973, Solar Phys., **31**, 55

Wilhelm, K., Curdt, W., Marsch, E., et al. 1995, Solar Phys., **162**, 189

Fig. 1.— This figure illustrates the key features and measures used in this paper to characterize chromospheric oscillation wave-packets. In panel a) we show a thumbnail image of the TRACE FOV (set # 4) and an asterisk marking the location of our sample timeseries. In panel b) we show the wavelet power spectrum with 95 % confidence inside the black contours. In Panel c) we show the "global wavelet power spectrum", the mean wavelet power averaged over time, from which we measure the mean packet frequency. In panel d) we show the 3-8 mHz average of the wavelet power and the average power of the 95% confidence contours. We use the intersection of the latter with the 3-8 mHz average power to mark the temporal boundaries of the packets (the finely cross-hatched areas) and consequently define the packet duration and time between packets or the packet "wait-time".

Fig. 2.— Packet parameter histogram samples from the longest frame sequence available, that of the JOP97 sunspot data, September 22, 2000 (# 7). At the top of this figure we show, from left to right, the imaging context for the timeseries in the form of the time averaged SOHO/MDI $B_{||}$ and TRACE 1700Å continuum intensity maps. Between these two we show the various masks that are defined to delineate the inter-network (white), network(grey), a buffer between them (dark grey) and the sunspot (black) regions as defined in Sect. 4. In the lower set of panels we present the packet parameter distributions for each of these regions; a) the mean packet frequency ν_X, b) the number of packets N_x, c) the packet duration D_x and d) the packet wait-time Δt_x.

Fig. 3.— From top to bottom we show the packet frequency, ν_X, the number of packets per hour, $\hat{N_X}$, the packet duration, D_X, wait-time, Δt_X, and the number of oscillation periods per packet $\hat{P_X}$ and their variation with the mean unsigned network magnetic field B^*. In each panel we show the network (dark) and inter-network (light) parameters, their variances and the best-fit straight line to the points. We also show the network (M_N) and inter-network (M_I) best-fit line gradients.

Fig. 4.— Spatial dependence of the TRACE packet parameters derived from the JOP72 full FOV data of February 26, 1999 (# 4). In the center and right columns we demonstrate the spatial behavior of the packet parameters beside those of the mean TRACE 1700Å continuum intensity (top left panel) and the MDI Mean line-of-sight magnetic field strength $B_{||}$ (bottom left panel). Many of the features discussed in the text and shown in Tab. 1 are clear.

Fig. 5.— Spatial dependence of the TRACE packet parameters derived from the JOP97 full FOV data of September 22, 2000 (# 7). See Fig. 4 for panel details.

Fig. 6.— Scatter plots showing the variations of the four packet parameters as a function of the $|B_{||}|$ for the JOP97 sunspot data of September 22, 2000 (# 7) of Figs. 2 and 5. We can clearly see the origin of the bimodal packet parameter distributions in the separation of the inter-network and network values. The transition of the packet parameters between these defined regions points to the influence of the intermediate magnetic region or magnetic "canopy" (gray shaded region).

Fig. 7.— Cartoon visualizations of the plasma topography in the strong and weak-field cases. In each visualization we show the field topology (multi-colored solid lines), the plasma-$\beta = 1$ iso-contour (thick gray band), an estimate of the vertical position of the TRACE 1700Å continuum formation layer (green gridded surface) and the planar total (gas+magnetic) pressure isobars which correspond to the topographic locations where 5-minute (solid thick black line), 4-minute (solid thick green line) and 3-minute (solid thick blue line) period waves form the characteristic period of oscillation.

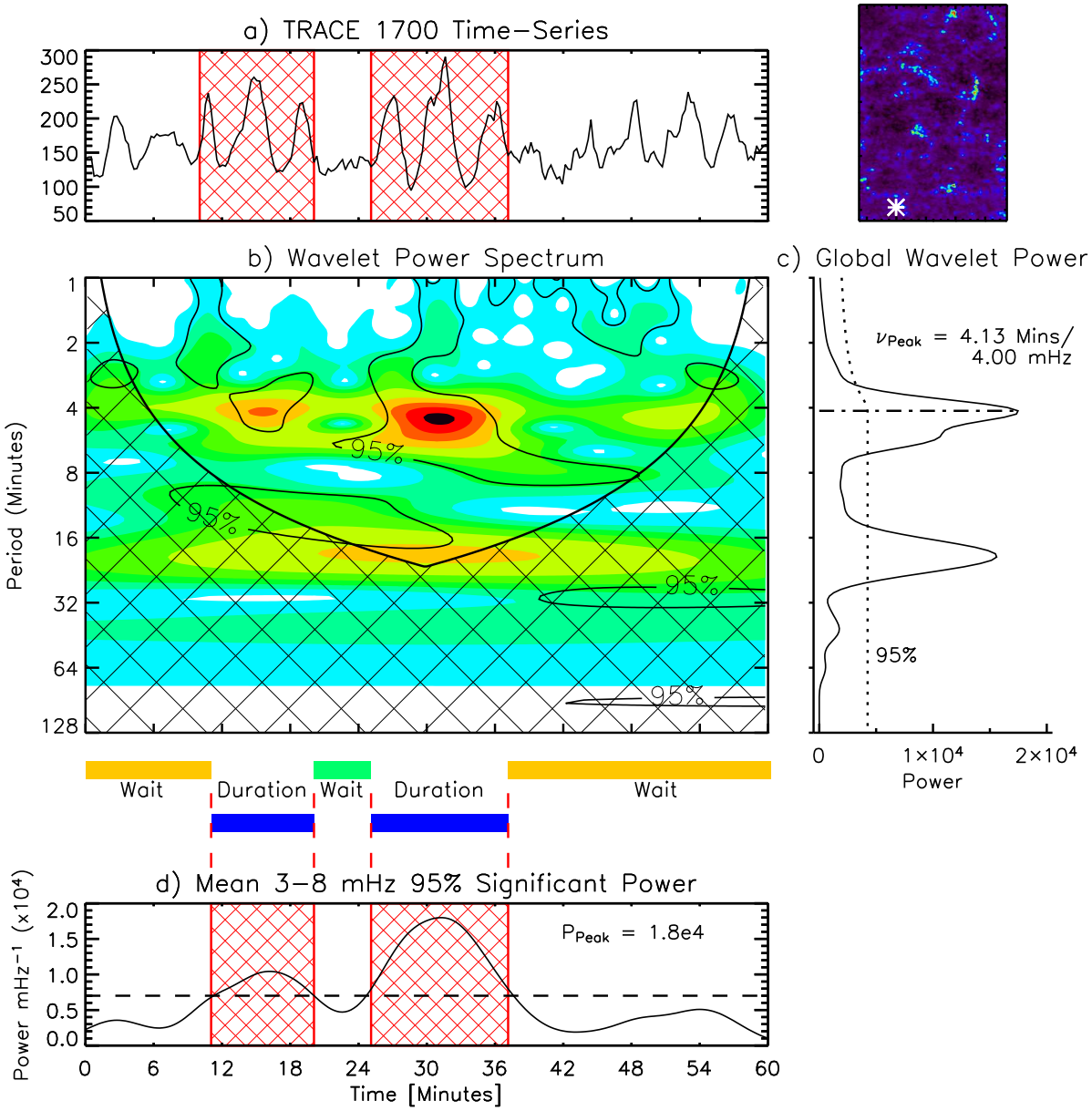
a) TRACE 1700 Time–Series
300
250
200
150
100
50
b) Wavelet Power Spectrum
c) Global Wavelet Power
Period (Minutes)
1
2
4
8
16
32
64
128
95%
95%
95%
95%
ν_{Peak} = 4.13 Mins/
4.00 mHz
95%
0
1×10⁴
2×10⁴
Power
Wait
Duration
Wait
Duration
Wait
d) Mean 3–8 mHz 95% Significant Power
Power mHz⁻¹ (x10⁴)
2.0
1.5
1.0
0.5
0.0
P_{Peak} = 1.8e4
0
6
12
18
24
30
36
42
48
54
60
Time [Minutes]

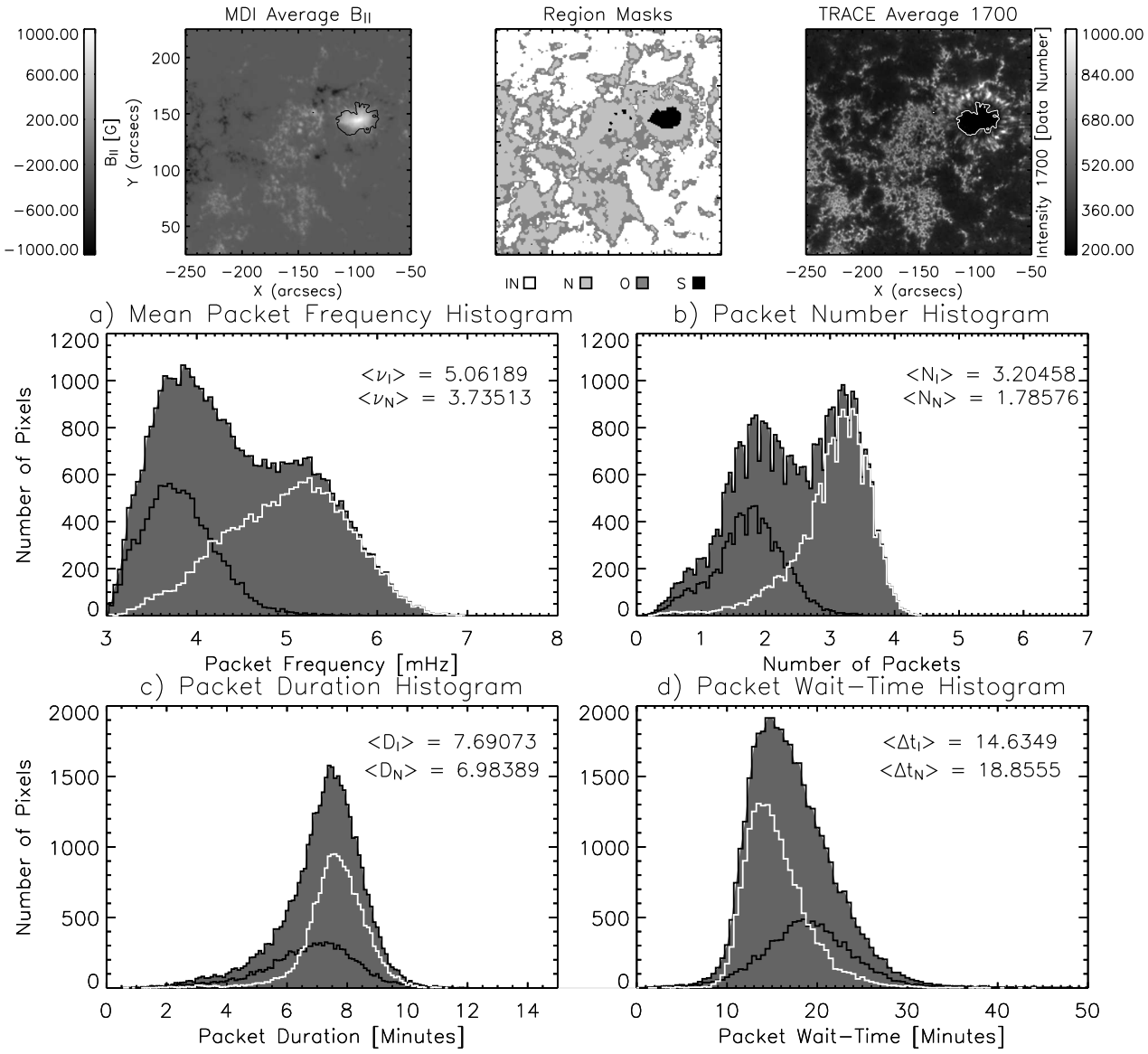
MDI Average B||
Region Masks
TRACE Average 1700
B|| [G]
Y (arcsecs)
X (arcsecs)
Intensity 1700 [Data Number]
IN N O S
a) Mean Packet Frequency Histogram
<ν_I> = 5.06189
<ν_N> = 3.73513
Number of Pixels
Packet Frequency [mHz]
b) Packet Number Histogram
<N_I> = 3.20458
<N_N> = 1.78576
Number of Packets
c) Packet Duration Histogram
<D_I> = 7.69073
<D_N> = 6.98389
Packet Duration [Minutes]
d) Packet Wait−Time Histogram
<Δt_I> = 14.6349
<Δt_N> = 18.8555
Packet Wait−Time [Minutes]

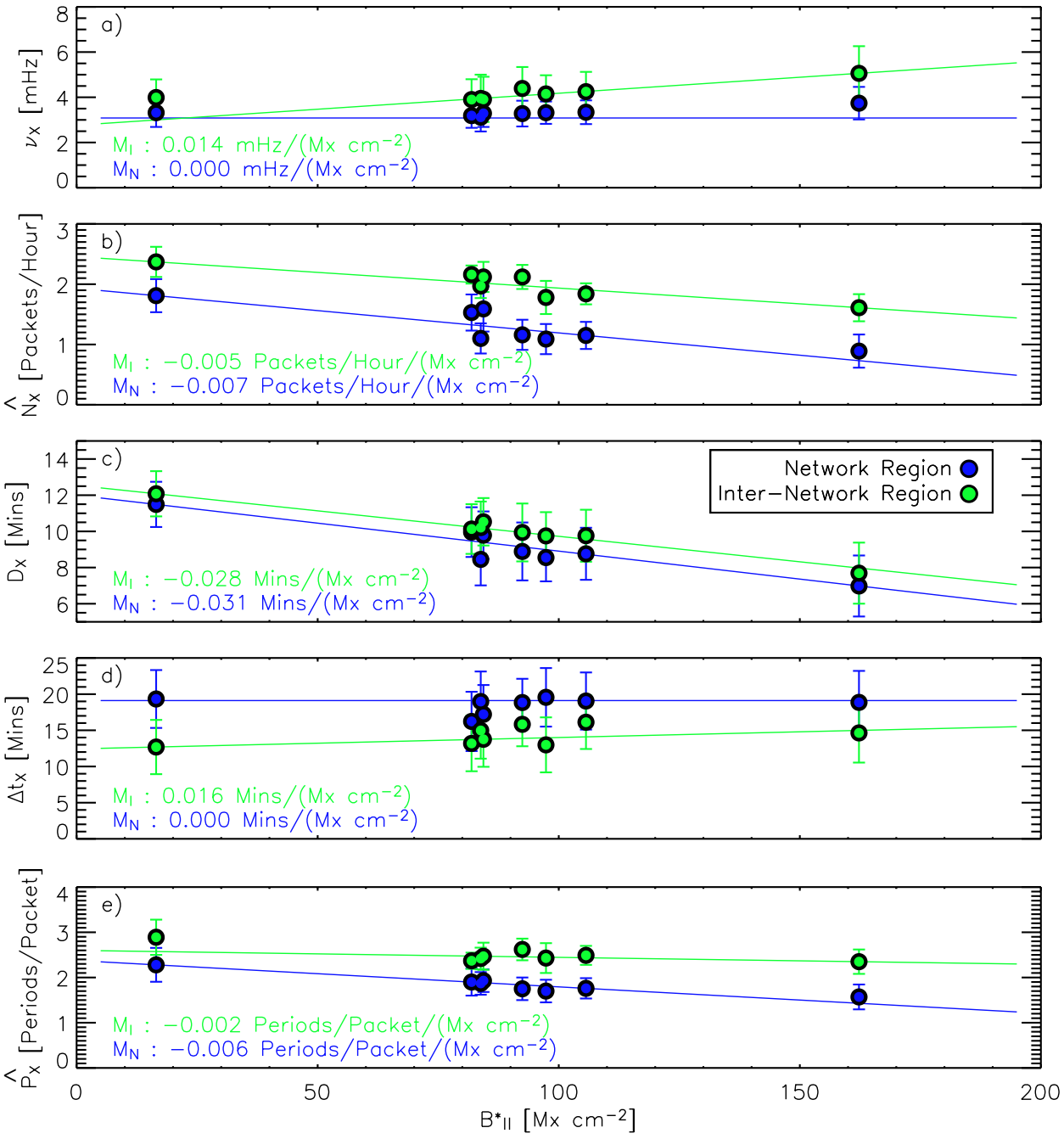
a)
ν_X [mHz]
M_I : 0.014 mHz/(Mx cm^{-2})
M_N : 0.000 mHz/(Mx cm^{-2})
b)
$\hat{N}_X$ [Packets/Hour]
M_I : −0.005 Packets/Hour/(Mx cm^{-2})
M_N : −0.007 Packets/Hour/(Mx cm^{-2})
c)
D_X [Mins]
Network Region
Inter−Network Region
M_I : −0.028 Mins/(Mx cm^{-2})
M_N : −0.031 Mins/(Mx cm^{-2})
d)
Δt_X [Mins]
M_I : 0.016 Mins/(Mx cm^{-2})
M_N : 0.000 Mins/(Mx cm^{-2})
e)
$\hat{P}_X$ [Periods/Packet]
M_I : −0.002 Periods/Packet/(Mx cm^{-2})
M_N : −0.006 Periods/Packet/(Mx cm^{-2})
0
50
100
150
200
B^*_{II} [Mx cm^{-2}]

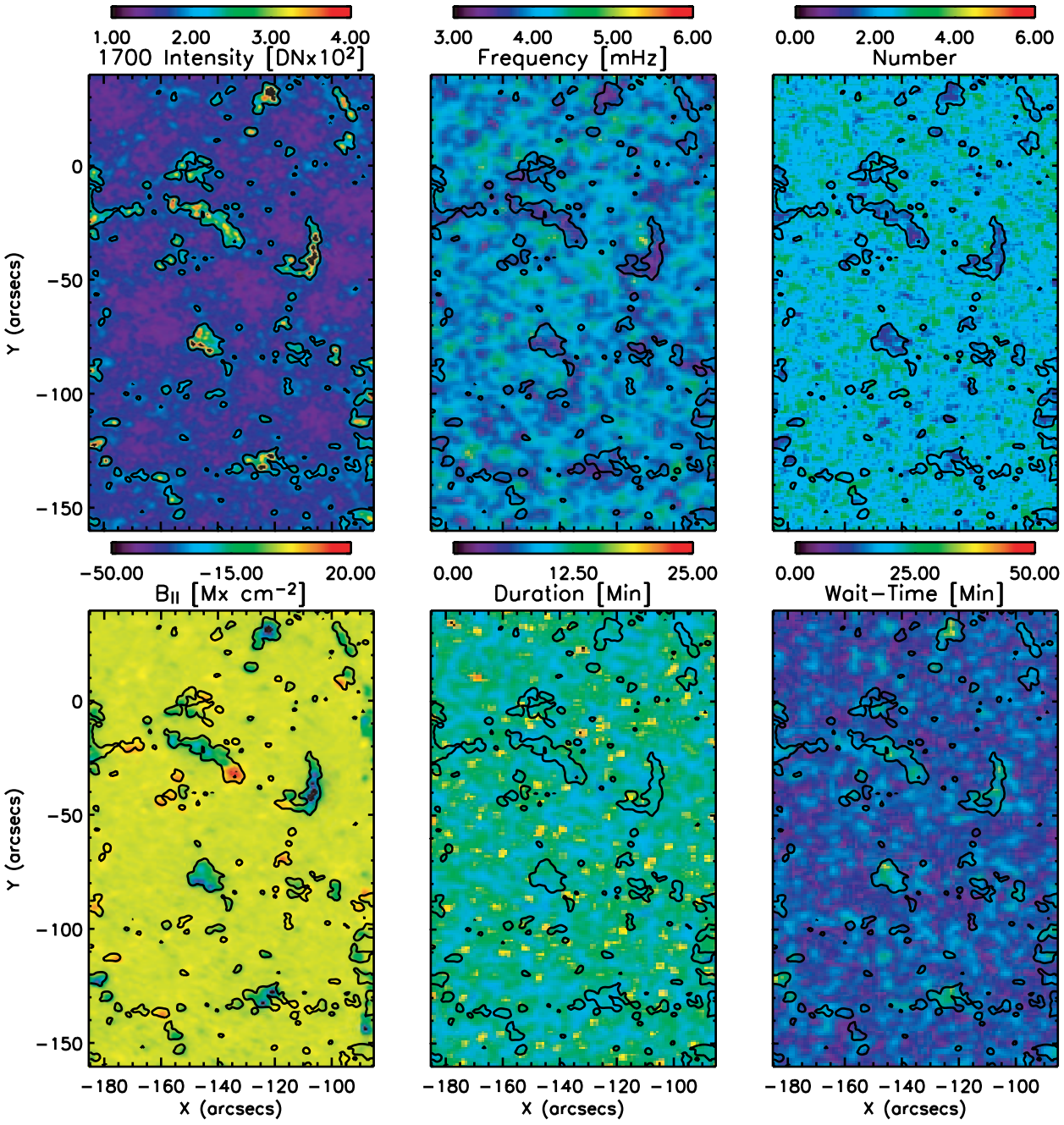
1.00 2.00 3.00 4.00
1700 Intensity [DNx10²]
3.00 4.00 5.00 6.00
Frequency [mHz]
0.00 2.00 4.00 6.00
Number
−50.00 −15.00 20.00
B|| [Mx cm⁻²]
0.00 12.50 25.00
Duration [Min]
0.00 25.00 50.00
Wait−Time [Min]
Y (arcsecs)
0
−50
−100
−150
−180 −160 −140 −120 −100
X (arcsecs)

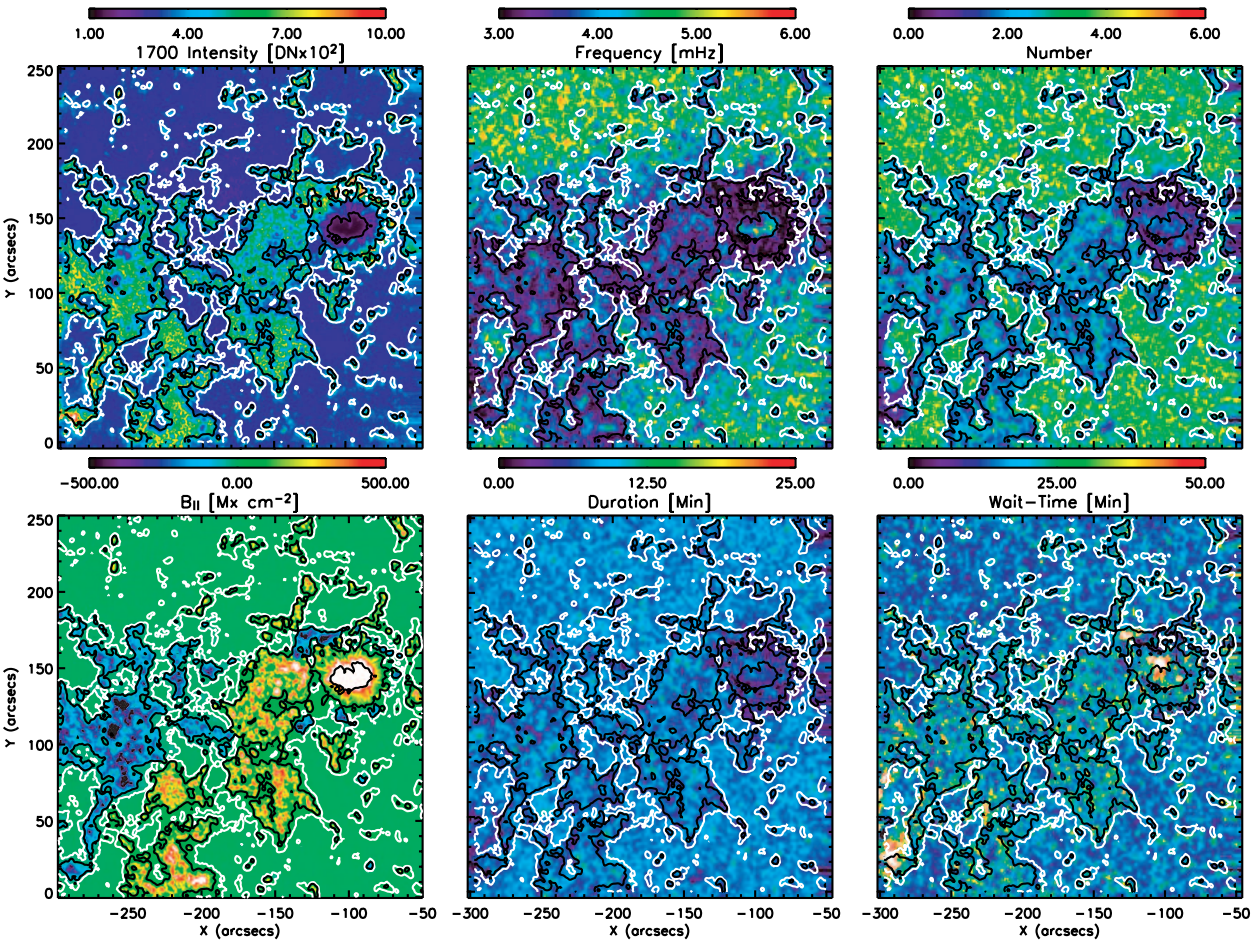
1.00
4.00
7.00
10.00
1700 Intensity [DNx10²]
3.00
4.00
5.00
6.00
Frequency [mHz]
0.00
2.00
4.00
6.00
Number
−500.00
0.00
500.00
B|| [Mx cm⁻²]
0.00
12.50
25.00
Duration [Min]
0.00
25.00
50.00
Wait−Time [Min]
Y (arcsecs)
X (arcsecs)
0
50
100
150
200
250
−250
−200
−150
−100
−50
−300

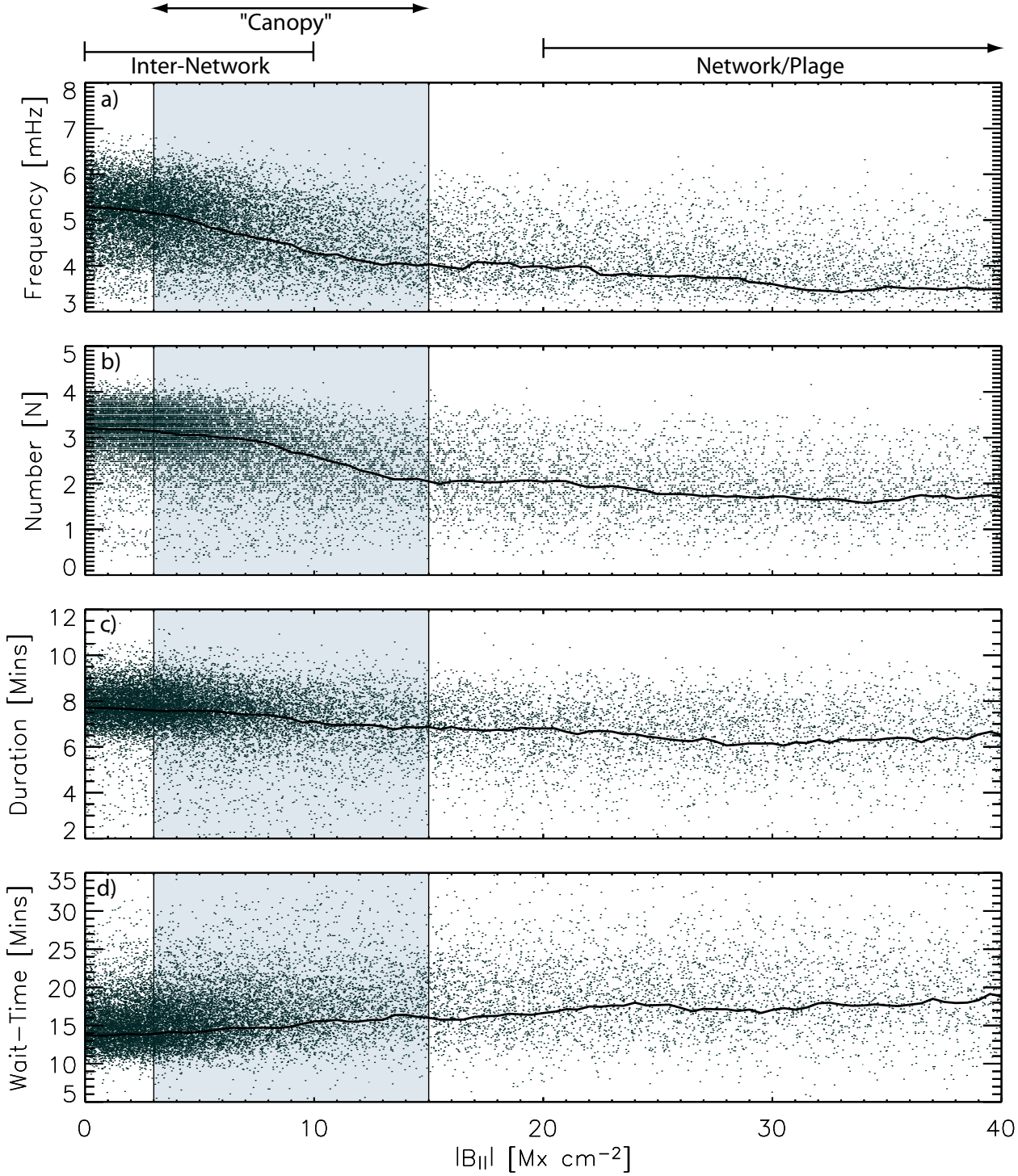
"Canopy"
Inter-Network
Network/Plage
a)
b)
c)
d)
Frequency [mHz]
Number [N]
Duration [Mins]
Wait−Time [Mins]
|B||| [Mx cm−2]

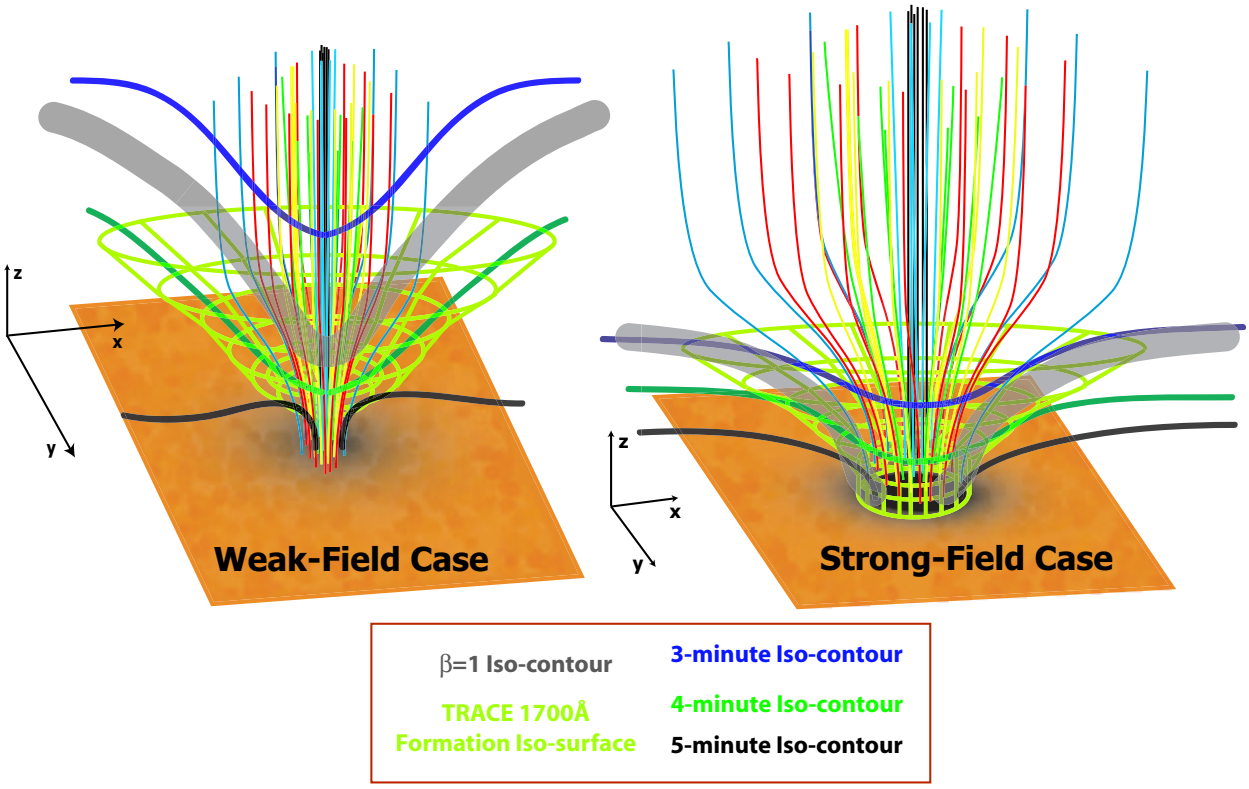
z
x
y
Weak-Field Case
z
x
y
Strong-Field Case
β=1 Iso-contour
TRACE 1700Å
Formation Iso-surface
3-minute Iso-contour
4-minute Iso-contour
5-minute Iso-contour

Table 1: Details of the packet distributions observed in the eight TRACE 1700Å continua timeseries datasets studied. Each dataset has an index, when the timeseries commenced, the number of frames in the sequence (n_f) with the time between images in this set fixed (dt = 15s), the mean unsigned network magnetic field strength (B^* in Mx cm^{-2}) and the mean packet parameters of region X discussed in the text (N_X, $\hat{N_X}$, ν_X, D_X, Δt_X, $\hat{P_X}$). The subscript X indicates where the packets were observed; $X = I$ in the inter-network and $X = N$ in network regions.

#	Date	T_0	n_f	B^*	N_N	$\hat{N_N}$	ν_N	D_N	Δt_N	$\hat{P_N}$	N_I	$\hat{N_I}$	ν_I	D_I	Δt_I	$\hat{P_I}$
1	1998/05/12	14:31	353	84.38	2.34	1.59	3.29	9.79	17.21	1.93	3.12	2.12	3.91	10.53	13.76	2.47
2	1998/05/16	14:33	345	81.92	2.20	1.53	3.19	9.96	16.23	1.90	3.11	2.16	3.90	10.13	13.19	2.37
3	1999/02/25	23:05	478	83.82	2.19	1.10	3.21	8.45	18.98	1.87	3.92	1.97	3.95	10.21	14.98	2.42
4	1999/02/26	23:00	239	16.50	1.81	1.81	3.32	11.49	19.33	2.29	2.36	2.36	3.99	12.08	12.69	2.89
5	1999/09/11	08:03	444	92.44	2.15	1.16	3.28	8.89	18.84	1.75	3.94	2.12	4.39	9.94	15.83	2.62
6	1999/09/13	08:02	464	105.65	2.24	1.15	3.34	8.76	19.05	1.76	3.56	1.84	4.25	9.76	16.12	2.49
7	2000/09/22	08:00	478	162.27	1.78	0.89	3.74	6.98	18.86	1.57	3.20	1.61	5.06	7.69	14.64	2.35
8	2001/08/17	23:00	430	97.35	1.96	1.09	3.32	8.55	19.56	1.70	3.19	1.78	4.15	9.75	12.99	2.43

Table 2: Inter-network packet details from the combined analysis of the JOP72 SOHO MDI/SUMER and TRACE observations of 1999 February 26 (# 4). We identify the observable, an estimate of where the signal is formed, the four inter-network packet parameters, the number of periods per packet and their associated errors (derived as standard deviations of the distributions).

Observable	Z (Mm)	N_I	ν_I	D_I	Δt_I	$\hat{P_I}$
MDI $V_{\|\|}$	0.2	2.41 ± 0.43	3.38 ± 0.16	12.87 ± 3.01	11.78 ± 4.12	2.61 ± 0.44
TRACE 1700Å	0.4-0.6	2.36 ± 0.37	3.99 ± 0.28	12.08 ± 2.25	12.69 ± 4.15	2.89 ± 0.29
TRACE 1600Å	0.4-0.6	2.36 ± 0.37	4.07 ± 0.31	11.80 ± 2.17	12.40 ± 3.92	2.88 ± 0.28
TRACE 1550Å	0.4-0.6	2.34 ± 0.67	4.08 ± 0.31	11.77 ± 2.22	12.51 ± 3.98	2.88 ± 0.31
SUMER continuum	0.7-1.2	2.36 ± 0.42	4.37 ± 0.92	10.01 ± 3.08	12.45 ± 5.91	2.43 ± 0.39
SUMER V N I 1199.55Å	1.0-2.0	2.50 ± 0.52	4.36 ± 1.07	8.83 ± 5.29	12.20 ± 5.16	2.44 ± 0.41
SUMER V N I 1200.22Å	1.0-2.0	2.53 ± 0.56	4.38 ± 1.05	8.87 ± 5.20	12.29 ± 5.24	2.43 ± 0.32
SUMER V Si II 1197.40Å	1.0-2.0	2.54 ± 0.92	4.64 ± 1.30	8.22 ± 3.27	11.58 ± 5.90	2.36 ± 0.36
SUMER V Si III 1206.51Å	1.0-2.0	2.69 ± 0.83	4.87 ± 0.78	7.75 ± 2.62	11.87 ± 6.24	2.26 ± 0.42